Smart Materials and Structures

PAPER

The effect of stress-induced martensite aging in tension and compression on B2–B19′ martensitic transformation in $Ni_{50.3}Ti_{32.2}Hf_{17.5}$ high-temperature shape memory alloy

IOP Publishing Smart Materials and Structures
Smart Mater. Struct. **30** (2021) 025039 (10pp) https://doi.org/10.1088/1361-665X/abdaa8

The effect of stress-induced martensite aging in tension and compression on B2–B19′ martensitic transformation in $Ni_{50.3}Ti_{32.2}Hf_{17.5}$ high-temperature shape memory alloy

A I Tagiltsev[1], E Yu Panchenko[1], E E Timofeeva[1], Yu I Chumlyakov[1], I D Fatkullin[1], E S Marchenko[1] and I Karaman[2]

[1] Tomsk State University, Lenina Str. 36, 634050 Tomsk, Russia
[2] Texas A&M University, College Station, TX 77843, United States of America

E-mail: antontgl@mail.tsu.ru

Received 24 August 2020, revised 29 November 2020
Accepted for publication 5 January 2021
Published 25 January 2021

Abstract

The present study investigates the high-temperature shape memory effect (SME) in heterophase $Ni_{50.3}Ti_{32.2}Hf_{17.5}$ polycrystals with nanosized *H*-phase particles after stress-induced martensite (SIM) aging in tension and compression. SIM aging created the conditions for fully reversible two-way SME with a strain of up to 50% of the one-way shape memory strain. SIM aging altered the viscoelastic properties of material, in particular, the elastic moduli of austenite and martensite increased, as did internal friction. Increased interface mobility is suggested as the reason for internal friction growth.

Keywords: shape memory alloy, martensitic transformation, stress-induced martensite aging, two-way shape memory effect

(Some figures may appear in colour only in the online journal)

1. Introduction

NiTiHf alloys with shape memory effect (SME) have been already known as a reliable, high-temperature ($T > 373$ K) materials. This makes them applicable to various applications such as actuators, sensors, detectors, complex operating mechanisms, and dampers [1, 2].

However, functional properties and alloy strength must be improved for its application at high-stress and high-temperature conditions. It can be achieved by the reduction of grain size due to an extrusion of polycrystals and the precipitation of *H*-phase and *H*′-phase particles in NiTiHf poly- and single-crystals. Particle precipitation allows for the control of functional properties for enhanced stability during thermal-induced B2–B19′ martensitic transformations (MTs). Additional mechanical training, up to 1600 thermal cycles under stress, can induce a two-way SME (TWSME) [2]. To-date, extruded polycrystals with small grain size have received extensive research attention [1, 3] while relatively little is known of random-orientation polycrystals with larger grain size $d > 10$ μm. To attend to this gap, the present research investigates non-extruded polycrystals.

Stress-induced martensite aging (SIM-aging) is another method for controlling functional properties. Evidence demonstrates that it can increase strength [4], induce rubber-like behavior and a TWSME [5, 6]. This occurs through a redistribution of point defects and various types of atoms, in accordance with the symmetry of martensite [5] resulting in martensite stabilization. These processes are more effective in material in which $M_s/T_m > 0.2$ (M_s—MT start temperature, T_m—melting temperature) [5]. Thus, high-temperature NiTiHf alloys with $M_s/T_m > 0.2$, which are expected to

demonstrate strong martensite stabilization, are a priority in SIM-aging research. The potential effectiveness of SIM-aging has been demonstrated in CoNiAl, NiFeGa, and CoNiGa single crystals [5, 7, 8], however a thorough investigation into the effect of SIM-aging on the properties of NiTiHf alloys has yet to be conducted.

The current study investigates the effect of SIM-aging in tension and compression, on stress-induced MT in $Ni_{50.3}Ti_{32.2}Hf_{17.5}$ (at.%) polycrystals with dispersed particles.

In the present study, tension and compression were selected as the two stress states based on a well-known feature of TiNi shape memory alloys. TiNi shape memory alloys demonstrate strong asymmetry of functional properties according to stress state: a reversible strain, critical stresses of martensite formation, stress and thermal hysteresis, and a yield stress level of B2-phase [9–11]. However to-date, the asymmetry of functional properties has received little research attention in NiTiHf polycrystals [12, 13] and the effect of SIM-aging on this asymmetry has not been studied yet. Attending to this gap, the present study sought to contribute to the body of knowledge on thermoelastic MTs in heterophase NiTiHf alloys.

2. Material and methods

Initially, $Ni_{50.3}Ti_{32.2}Hf_{17.5}$ (at.%) polycrystals were electric-arc melted from components with high purity (99.99%). Samples with sizes of 20 × 1.5 × 2.5 mm^3 with dog-bone shape for tension and sizes of 3 × 3 × 6 mm^3 with parallelepiped shape for compression were cut. Before conducting experiments, samples were mechanically and electrically polished to remove the hardened surface layer. Average grain size was 36 μm; this was not affected by austenite or martensite aging.

Chemical composition was controlled by a wavelength dispersive x-ray fluorescence spectrometer XRF-1800. Composition corresponded to the nominal $Ni_{50.3}Ti_{32.2}Hf_{17.5}$ (at.%), with a margin of error of 5% of the measured value. This composition was selected according to previous findings [14], that the addition of 10 at.% of Hf did not influence MT temperatures, while 20–25 at.% induced plasticity reduction and the appearance of areas with undissolved Hf. Therefore, the composition of $Ni_{50.3}Ti_{32.2}Hf_{17.5}$ (at.%) was used to obtain suitable plasticity and high MT temperatures above 373 K.

The polycrystals were investigated after the following treatments: (a) stress-free austenite aging at 773 K, 3 h with subsequent cooling in air (initial crystals); (b) (a) + SIM-aging at 428 K for 12 h (SIM-aged crystals). Austenite aging was selected to induce precipitation of nanosized H-phase particles [15]. Regarding SIM-aging, it was performed at $T = 428$ K under a constant stress in the martensitic state. Initially, the sample was heated up to $T = 523$ K in stress-free state and then a stress σ_{app} was applied. The stress level of −400 MPa was applied to compressive samples and the stress level of 300 MPa was applied to tensile samples. These stresses were chosen to achieve maximum reversible strain while avoiding destruction of the tensile samples. Then the temperature was decreased to $T = 300$ K < M_f while σ_{app} was kept constant. Consequently, the forward B2–B19′ MT was induced. In the next step, the temperature was increased to $T = 428$ K to instigate the SIM-aging process. It should be noted, that this temperature though close but does not exceed A_s temperature, so the reverse MT is absent. So, the chosen temperature is the maximum temperature for thermodynamically stable SIM for both tension and compression samples. After the holding at $T = 428$ K, the temperature was increased to $T = 523$ K and the reverse B19′–B2 MT was observed. After that the sample was unloaded. The maximum time for aging in the martensitic state was selected according to whether, during the previous 3 h of aging, no change in $\varepsilon(T)$ curves of SME had been observed. Thereafter, the material was considered to be stable and the TWSME and SME were investigated. The investigations of SME were carried out after SIM-aging: under tension for tensile samples and under compression for compressive samples.

MT temperatures were obtained using a differential scanning calorimeter DSC 404 $F1$ in stress-free state. Mechanical tests and SIM-aging were carried out on dilatometer with obtaining the $\varepsilon(T)$ curves upon cooling/heating cycles in stress-free state (TWSME) and under applied constant stress (SME). The rate of cooling/heating in all experiments was 10 K min^{-1}. During analysis of experimental data, the measurement errors of strain ± 0.3%, temperature ±2 K, and stress ±2 MPa were taken into account. Transmission electron microscopy (TEM) studies were carried out on a CM-12 operated at an accelerating voltage of 120 kV.

The viscoelastic properties of material were analyzed using a testing machine for dynamic–mechanical analysis, DMA/SDTA 861e, under tension with a maximum strain of 10 μm (working length of 10 mm), and at frequencies of 0.1, 0.4, 1, 5, 10 Hz.

3. Results and discussion

3.1. Microstructure and thermally-induced MT

Figure 1 shows the results of TEM investigations of aged at 773 K, 3 h $Ni_{50.3}Ti_{32.2}Hf_{17.5}$ (at.%) polycrystals in initial state (figures 1(a) and (b)), and after SIM-aging in compression (figure 1(c)). Aging at 773 K, 3 h resulted in precipitation of dispersed H-phase particles. Figure 1(a) demonstrates reflexes from the B2-matrix and reflexes $^1/_2 < 111 > B2$ from the particles, typical for H-phase [16, 17]. Additional reflexes, ¼ < 111 > B2, typical for H'-phase, are not observed in the selected area electron diffraction pattern (SAEDP). H-phase has a face-centered orthorhombic lattice with parameters $a = 4a_0$, $b = 2\sqrt{2}a_0$, and $c = 6\sqrt{2}a_0$ [16, 17]. Average precipitate size was 10–15 nm.

Figure 1(b) presents the thermally-induced B19′-martensite which containing a high density of compound twins $(001)_{B19'}$, which reflexes are observed on SAEDP in initial polycrystals. The small precipitates are completely embedded in the martensite variants, which is in agreement with previous work [18] in which compound twins were contained by B19′-martensite, twinned by (011) type I.

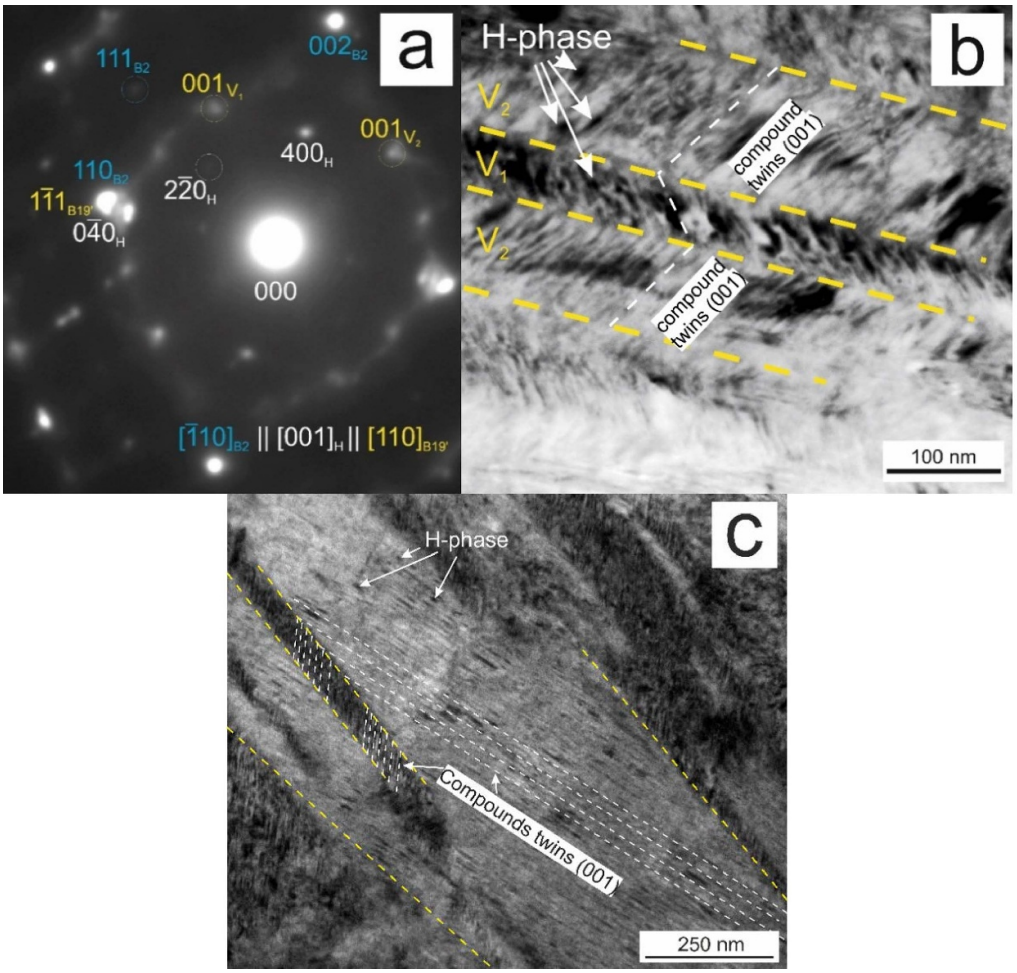

Figure 1. TEM images for $Ni_{50.3}Ti_{32.2}Hf_{17.5}$ polycrystals: SAEDP, zone axis $[\bar{1}10]_{B2} \parallel [001]_H \parallel [110]_{B19'}$ (a) and a corresponding bright-field image (b) of initial polycrystals; bright field image of SIM-aged in compression polycrystals (c).

SIM-aging did not affect the grain size of polycrystals or type of twinning, *H*-phase particles and a high density of compound $(001)_{B19'}$ twins were observed. However, it should be noted that the oriented martensite bands in sizes of up to 500 nm are observed after SIM-aging in comparison with non-oriented small bands in initial polycrystals (figures 1(b) and (c)).

Figures 2 and 3 show the dependence on temperature of both elastic modulus and internal friction in comparison with DSC curves in initial and SIM-aged in tension polycrystals.

The MT temperatures (M_s, M_f, A_s, and A_f) were determined by the tangent to the calorimetric curves; thermal hysteresis was determined as the difference between $\frac{M_s+M_f}{2}$ and $\frac{A_s+A_f}{2}$ temperatures (table 1). It was experimentally shown, that DSC data obtained for SIM-aged in tension and in compression samples is close to each other and does not exceed the measurement error of ± 2 K. The experimental values of MT temperatures approximate those obtained from $Ni_{50.3}Ti_{29.7}Hf_{20.0}$ (at.%) polycrystals extruded at 1173 K and aged at 773 K, 3 h [1].

The DMA results strongly correlate with DSC results on studies of B2–B19′ MTs at cooling/heating: the close peak temperatures of forward and reverse MT are observed. First, figures 2 and 3 demonstrate the asymmetry of peak temperatures on DMA and DSC curves in both initial and SIM-aged polycrystals; it appears as widening of MT intervals near the M_f and A_s temperatures. That is why the maximum peak temperatures (M_p and A_p) upon cooling and heating do not correspond to the average temperature of forward and reverse MT: $M_p \neq 1/2(M_s + M_f)$ and $A_p \neq 1/2(A_s + A_f)$. This is explained by the presence of both nanotwinned B19′-martensite and nanosized particles (figure 1), which promotes significant increase in elastic energy during forward MT, which consequently results in MT asymmetry. The same behavior has previously been observed in as-cast NiTiHf alloys [19], supports the reasoning that such asymmetry is associated with the same material's microstructure: twinned martensite with nanosized dispersed particles.

Second, from figures 2 and 3 it is evident that SIM-aging leads to increased elastic moduli in martensite and austenite. However, martensite elastic modulus increases more (34% from the initial value) than does the austenite one (15% from the initial value).

Third, following SIM-aging, elastic modulus softening at MT becomes more than three times stronger (from ~5 GPa

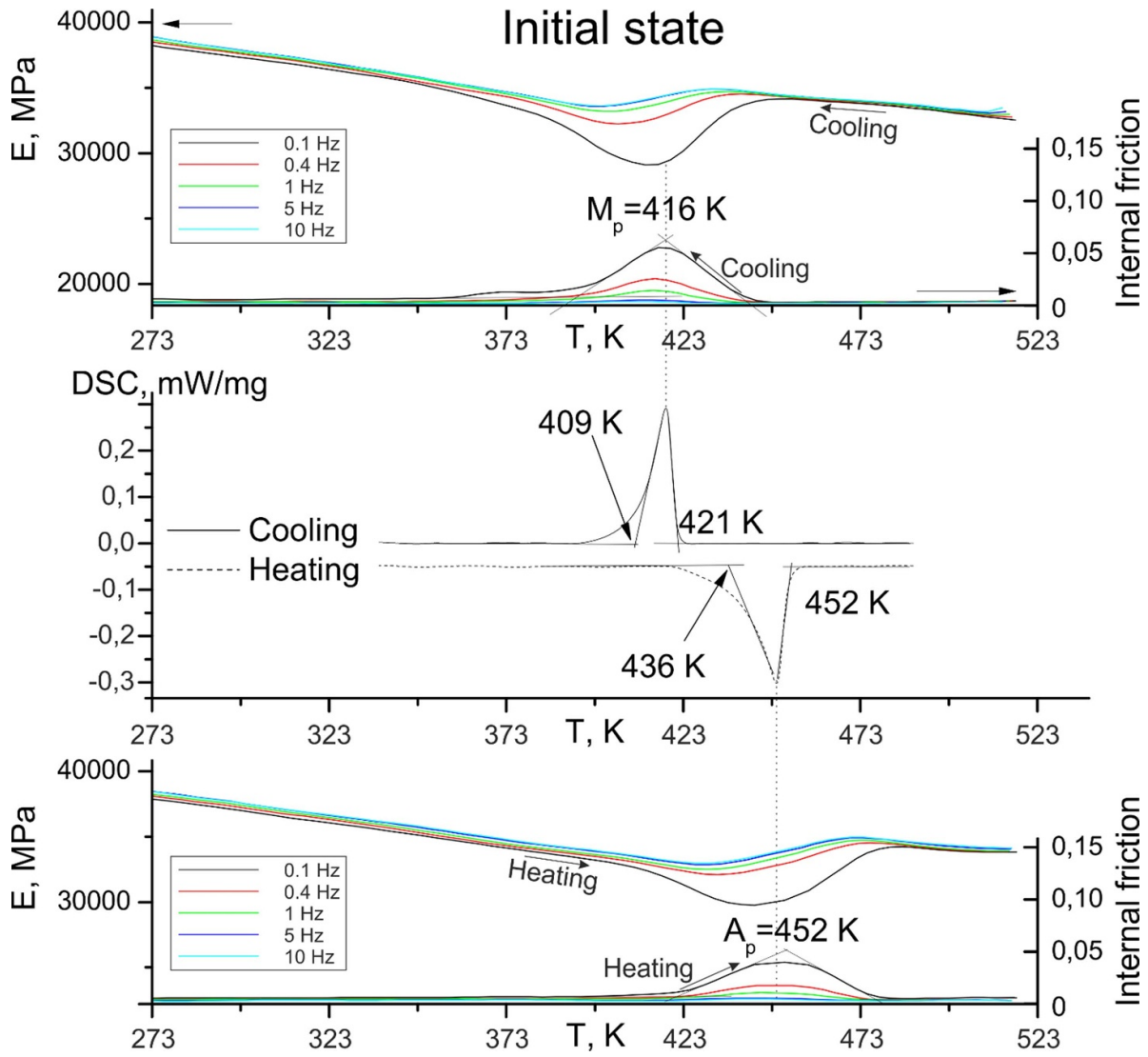

Figure 2. The dependence of elastic modulus and internal friction on temperature in tensile sample in comparison with DSC curves at cooling/heating for initial $Ni_{50.3}Ti_{32.2}Hf_{17.5}$ polycrystals.

Table 1. Characteristic properties obtained using DSC-curves in initial and SIM-aged in tension $Ni_{50.3}Ti_{32.2}Hf_{17.5}$ polycrystals.

	M_s, (±2)K	M_f, (±2)K	A_s, (±2)K	A_f, (±2)K	Δ_1, (±2)K	Δ_2, (±2)K	ΔT, (±2)K	$\Delta S_{cooling}$, J (kg × K)$^{-1}$	$\Delta S_{heating}$, J (kg × K)$^{-1}$
Initial state	421	409	439	452	12	13	29	−49,5	50.0
SIM-aged state in tension	421	401	436	452	20	16	34	−45,3	40,7

in initial state to ∼16.5 GPa after SIM-aging during forward MT) at a frequency of 0.1 Hz. Modulus softening is usual for shape memory alloys and is a feature of a pre-martensitic state [20]. Softening is characterized by a deviation from linear temperature dependence of elastic modulus and describes the rebuilding of crystal lattice: it becomes soft, amenable and easy to deform in order to create another phase. Softening in the present study is defined as the difference between the minimum value of elastic modulus during forward MT (at M_p peak temperature) and the maximum value of elastic modulus before non-linear behavior is observed. It also should be noted, that according to [21] such behavior of curves (figures 2 and 3) when the peak temperature does not depend on frequency is the evidence of MT.

Fourth, SIM-aging provides the growth of internal friction. Previous findings indicate that the maximum peaks of internal friction Q^{-1} are 0.023 and 0.015 for homogenized and subsequently quenched NiTiHf polycrystals at cooling and heating, respectively [22]. Such a low peak (in comparison with NiTi alloy) is associated with the low mobility of twinning/interphase boundaries in martensite.

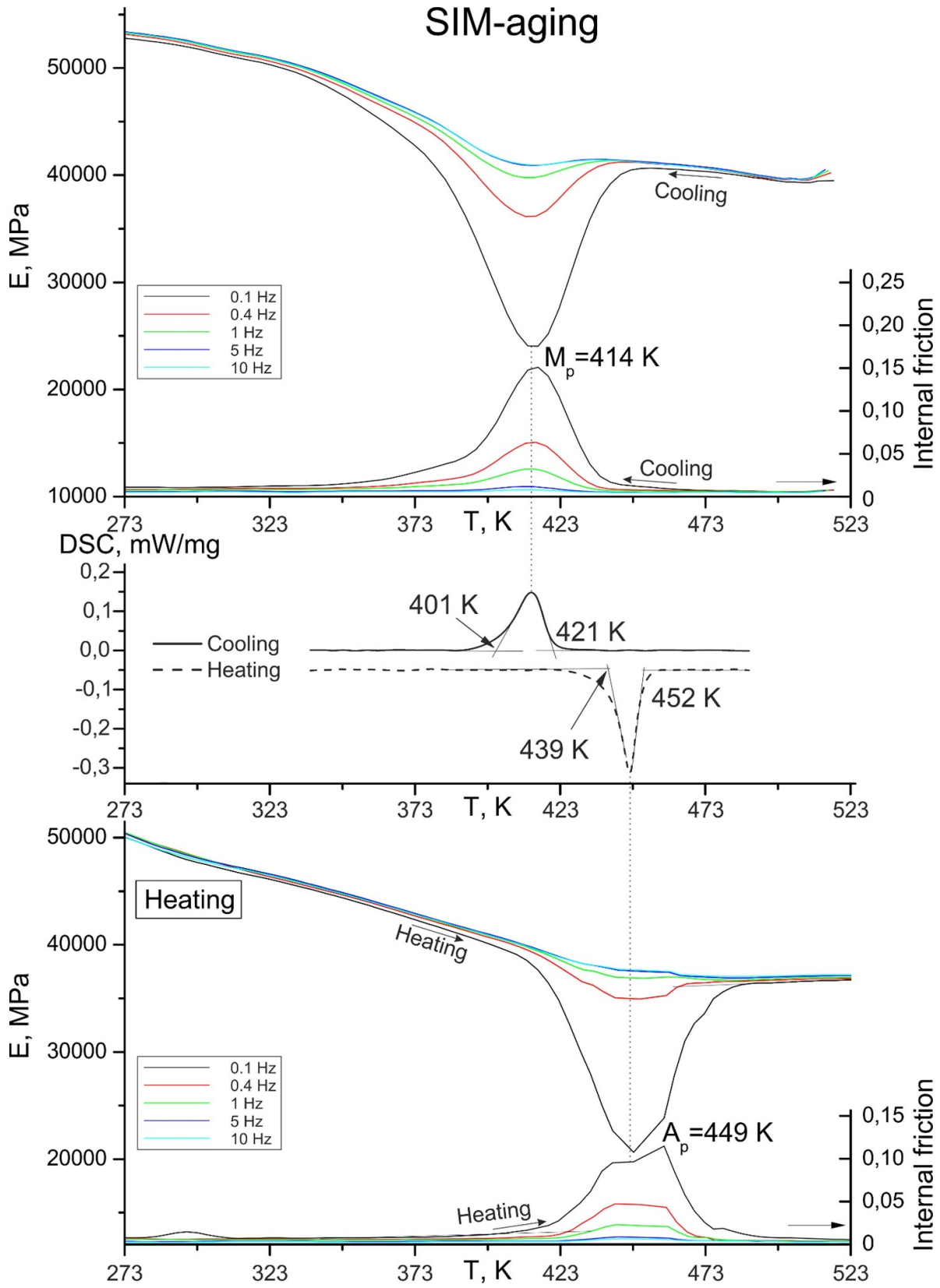

Figure 3. The dependence of elastic modulus and internal friction on temperature in tensile sample in comparison with DSC curves at cooling/heating for SIM-aged in tension $Ni_{50.3}Ti_{32.2}Hf_{17.5}$ polycrystals.

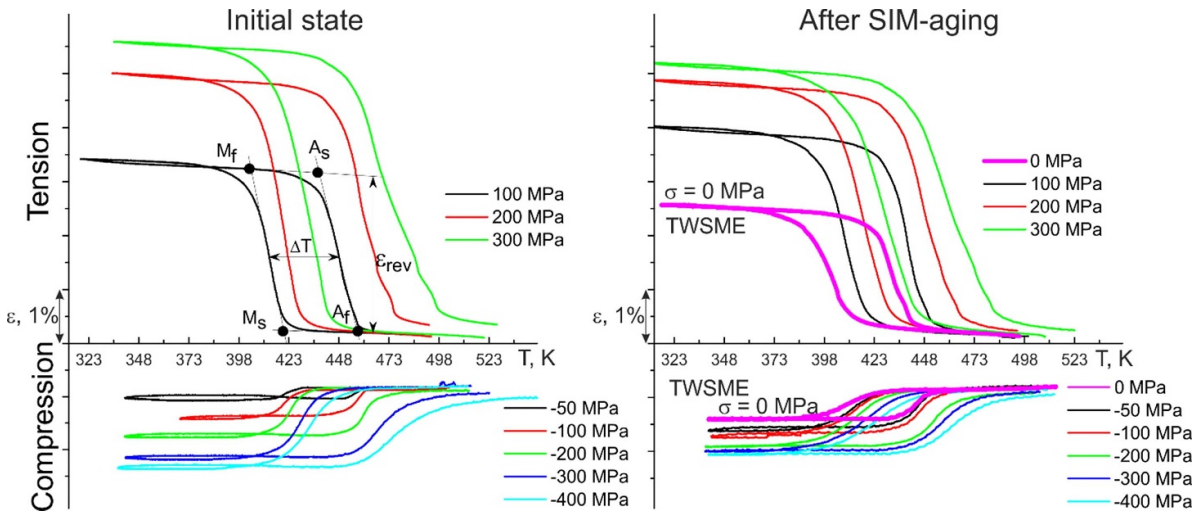

Figure 4. $\varepsilon(T)$ curves for initial and SIM-aged $Ni_{50.3}Ti_{32.2}Hf_{17.5}$ polycrystals in tension and compression.

In the present work, the initial polycrystals possessed almost the same values of internal friction (0.018 and 0.014) at a similar regime (frequency of 1 Hz). However, SIM-aging resulted in significant increase of internal friction, around double (up to 0.04 and 0.03), from the initial state. According to [22], internal friction growth is evidence of increased mobility of twinning/interphase boundaries. It is assumed, that such an effect is associated with increased compatibility between nanosized *H*-phase particles and twinned B19′-martensite during SIM-aging.

The *H*-phase particles are precipitated in austenite phase during aging at 773 K for 3 h and are inherited by martensite at MT. The high temperature of SIM-aging would provide the conditions for diffuse processes on the particle-matrix boundary. These conditions are not necessary for additional precipitation of *H*-phase, and SIM-aging effects only on the shape of *H*-phase particles. The fact that particles can change their shape under load at high temperature was confirmed by work [23]. So the subsequent stress-induced MT after SIM-aging occurs more easily, because the compatibility between nanosized particles and twinned SIM has increased. However, it is necessary to conduct additional TEM studies to explore its influence in NiTiHf polycrystals.

3.2. One-way and TWSME

In the present study, the self-accommodation structure was observed during B2–B19′ MT in the initial $Ni_{50.3}Ti_{32.2}Hf_{17.5}$ (at.%) polycrystals and the samples did not change their shape. On the contrary, in SIM-aged polycrystals TWSME was obtained with a reversible compressive strain of -0.6% (for compressive samples) and a reversible tensile strain of $+2.3\%$ (for tensile samples) (figure 4). Such asymmetry is associated with the asymmetry of lattice deformation at B2-B19′ MT ($+16.8\%$ in tension and -8.5% in compression) [9].

The TWSME tensile strain of $+2.3\%$ exceeds the known values of TWSME tensile strain obtained by mechanical trainings in NiTiHf alloys [24]. The maximum TWSME tensile strain was $+1.5\%$ in $Ni_{50.3}Ti_{29.7}Hf_{20}$ polycrystals after extrusion and training (100 thermal cycles under stress of 150 MPa). Aging at 823 K, 3 h, and training during 200 thermal cycles under a stress of 200 MPa, induced tensile TWSME with a strain of $+1.3\%$. Only high-cycling training (600 and 1600 cycles under stress of 145 MPa) was successful to receive large TWSME strain of up to 3%, and only under torsion [2].

It should be noted that TWSME usually appears in shape memory alloys due to the internal stress caused by irreversible strain over enduring trainings. However in the present study, the irreversibility after SIM-aging is low and so the induction of TWSME is assumed to be associated with the appearance of internal stress caused by two factors, the first being by rearrangement of point defects in structure and martensite stabilization. As it follows from [25], martensite stabilization is divided into chemical and mechanical, and correspondingly, the shift of TTs or the broadening of the reverse MT range is observed. The chemical stabilization of martensite consists of change in the short-range order of point defects and atoms in accordance with martensite symmetry, while mechanical stabilization in turn is caused by the pinning of interphase and/or twinning boundaries by dislocations and point defects. The second reason for TWSME induction can be associated with the change of compatibility: it increases between oriented martensite and nanosized H-phase particles during SIM-aging which in turn increases the mismatch between austenite and *H*-phase particles. It results in priority growth of oriented martensite upon cooling/heating cycles in stress-free state.

Thus, SIM-aging in tension and in compression, is an effective method for inducing TWSME in NiTiHf alloys.

When external stress was applied, SME was observed upon cooling/heating. TWSME in SIM-aged polycrystals promoted increased SME strain at low stress, in comparison with the initial aged polycrystals: from $+2.7\%$ to $+3.7\%$ at 100 MPa in tension, and from -0.2% to -0.75% at -50 MPa in compression (figure 4).

The reversible SME strain ε_{rev} reached maximum values with increased applied stress; SIM-aging did not affect the strain. Strong tension/compression asymmetry of maximum

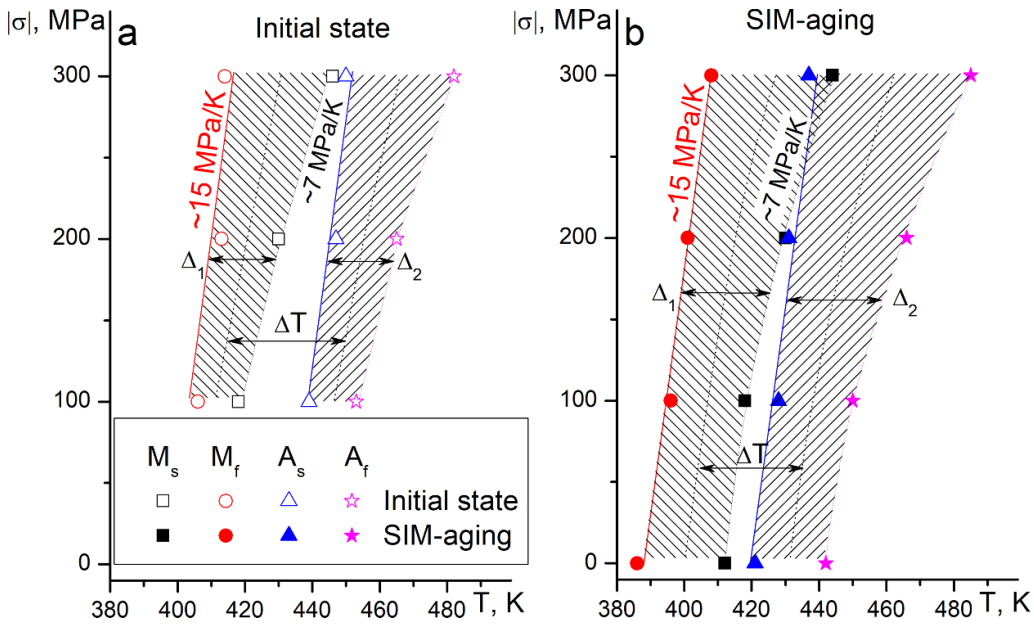

Figure 5. The $(\sigma-T)$ dependence for initial and SIM-aged $Ni_{50.3}Ti_{32.2}Hf_{17.5}$ polycrystals for tensile samples.

reversible strain during SME is observed before and after SIM-aging. The maximum compressive reversible strain of -1.3% during stress-assisted cooling/heating was obtained at -400 MPa, while the maximum tensile reversible strain was $+5.0\%$ at 300 MPa. Further applied stress led to decreased reversible strain, the appearance of irreversible strain, and destruction of tensile samples.

It should be noted, that the full resource of the lattice strain ($+16.8\%$ in tension and -8.5% in compression) has never been observed experimentally in NiTiHf alloy and only local areas are known, in which the experimental reversible strain achieves theoretical values in both polycrystals and single crystals [9]. The maximum reversible strain obtained strongly depends on microstructure of polycrystals [10, 26–28]: the grain size, the presence of texture after extrusion, the size and volume fraction of H-phase particles that do not undergo MTs and the chemical composition. In present work the experimentally obtained reversible strain in random-oriented polycrystals with large grain size (36 μm) can be compared with the strain in extruded and subsequently aged polycrystals. According to previous works [13] the experimental reversible strain in extruded $Ni_{50.3}Ti_{29.7}Hf_{20}$ polycrystals achieves $+(3.9 \div 4.8)\%$ in tension and $-(2.1 \div 3.5)\%$ in compression. These results are in accordance with the reversible strain obtained in tension ($+5.0\%$) in present work. However, the reversible strain of -1.3% in compression was substantially smaller than the experimental data of -3.5% in [13]. Such behavior can be explained by several factors. First, the polycrystals with large grain size possess lower strength properties compared with the extruded nanocrystalline polycrystals. Second, it was shown [10] that the critical stress level of oriented martensite formation strongly depends on deformation way in TiNi-based polycrystals: the higher stress level is required to form martensite in compression. Hence, during MT in compression the stress level achieves materials strength properties resulting in observation of plastic deformation and low reversible strain. On the other hand, the low stress level in tension does not reach strength properties during MT. This is the reason why in such polycrystals the MT at cooling/heating in compression is accompanied by irreversible strain before reaching the maximum strain. However, in tension it is possible to obtain the maximum reversible strain at 300 MPa as well as in other works [13].

It also should be noted that so small reversible strain obtained in present work in compression is corresponded to obtained strain in non-extruded aged Ni-rich $Ni_{51.2}Ti_{28.8}Hf_{20}$ (at.%) polycrystals [29]: the reversible strain of -1.2% is obtained in compression under stress level of -500 MPa, and the maximum strain of -1.8% can be achieved under compressive stress of -900 MPa, because the increased content of Ni results in the rise of materials strength properties.

3.3. SIM-aging effects on the properties changes

The dependence of transformation temperature on applied stress level in accordance with $\varepsilon(T)$ curves, are presented in figures 5 and 6 for initial and SIM-aged NiTiHf polycrystals in tension and compression. It is evident that forward and reversed MT temperature increases with greater applied stress. This is caused by increased chemical equilibrium T_0 temperature in accordance with Clapeyron–Clausius equation [30]:

$$T_0(\sigma) = T_0(0) + \sigma V \varepsilon_{tr} - \Delta s, \qquad (1)$$

where Δs is an entropy change, V is a molar volume, T and σ are temperature and stress level, and ε_{tr} is a transformation strain. The coefficient $\alpha = d\sigma\, dT^{-1}$ describes increased stress with increased temperature, and is inversely proportional to transformation strain ε_{tr}. This depicts the dependence

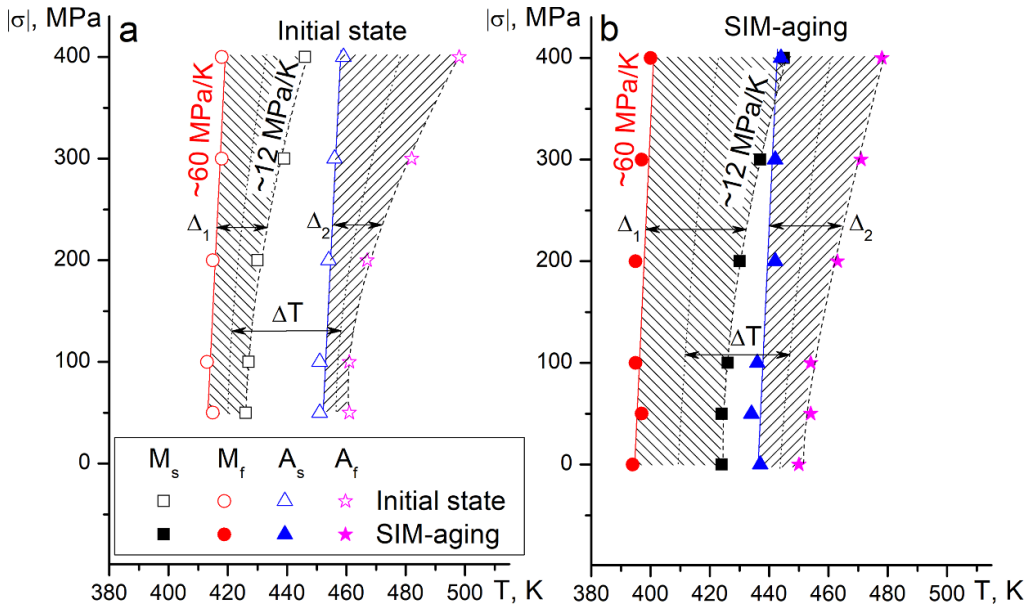

Figure 6. The $(\sigma-T)$ dependence for initial and SIM-aged $Ni_{50.3}Ti_{32.2}Hf_{17.5}$ polycrystals for compressive samples.

of $\alpha = d\sigma\ dT^{-1}$ on the stress state: as the ε_{tr} value in tension is much higher than in compression (figure 4), the $\alpha = d\sigma\ dT^{-1}$ is lower in tension compared to compression. Such behavior is common for shape memory alloys and is observed in both initial and SIM-aged polycrystals [12, 13].

However, the values of $\alpha = d\sigma\ dT^{-1}$ for M_f and A_s transformation temperatures are higher than for M_s and A_f temperatures that have non-linear temperature dependence on applied stress (figures 5 and 6). Therefore, the underlying mechanism dictating transformation temperatures is complex and it is necessary to take into account the effect of oriented martensite volume fraction ξ on both the transformation strain ε_{tr} and on the nonchemical contribution of energy of stress-induced MT.

Descriptions of transformation temperature changes as externally applied stress in accordance with local equilibrium formalism are taken into account [25, 31], are written as follows:

$$M_s(\sigma) = T_0(\sigma) - \frac{\left(d_{\xi=0}^{A\to M} + e_{\xi=0}^{A\to M}\right)}{-\Delta s}, \tag{2}$$

$$M_f(\sigma) = T_0(\sigma) - \frac{\left(d_{\xi=1}^{A\to M}(\xi) + e_{\xi=1}^{A\to M}(\xi)\right)}{-\Delta s}, \tag{3}$$

$$A_f(\sigma) = T(\sigma) + \frac{\left(d_{\xi=o}^{M\to A} - e_{\xi=o}^{M\to A}\right)}{-\Delta s}, \tag{4}$$

$$A_s(\sigma) = T_0(\sigma) + \frac{\left(d_{\xi=1}^{M\to A}(\xi) - e_{\xi=1}^{M\to A}(\xi)\right)}{-\Delta s}, \tag{5}$$

where ξ is the volume fraction of oriented martensite, M and A indexes are the designations of martensite and austenite phases, and e and d are the derivatives of the elastic and dissipative energies towards the volume fraction of transformed martensite.

At low applied stress levels, $\sigma < 300$ MPa, the transformation strain is lower than the theoretical strain $\varepsilon_{tr} < \varepsilon_{tr}{}^0$ and depends on the applied stress $\varepsilon_{tr} = \varepsilon_{tr}(\sigma)$. Therefore, the coefficient $\alpha = d\sigma\ dT^{-1}$ will reduce with increased stress, as the transformation strain $\varepsilon_{tr}(\sigma)$ will increase. For this reason, high values of $\alpha = d\sigma\ dT^{-1} > 15$ MPa K^{-1} are obtained at low applied stress when the transformation strain is small. Increased applied stress promotes change of $\alpha = d\sigma/dT$ until the stress, at which both the volume fraction of martensite and the transformation strain are at maximum, was achieved. Similar behavior was observed in $Ni_{50.3}Ti_{37.2}Hf_{12.5}$ polycrystals [32] in which transformation strain change significantly affected the coefficient $\alpha = d\sigma\ dT^{-1}$ of M_s temperature.

The second reason for the non-linear behavior of transformation temperatures is the dependence of elastic e and d dissipative energy on the volume fraction of oriented martensite ξ. It should be noted that the elastic energy value at the end of MT (when $\xi\to1$) is much higher than at the start of MT (when $\xi\to0$): $e_{\xi=1}^{A\to M} \gg e_{\xi=0}^{A\to M}$. A significant increase of elastic energy at $\xi\to1$ is common for high-strength alloys containing dispersed particles. Such increase of elastic energy results in additional decrease of M_f and A_s temperatures, in comparison with M_s and A_f temperatures in which the $e_{\xi=0}^{A\to M}$ is low, as follows from (2)–(5).

Different coefficients $\alpha = d\sigma\ dT^{-1}$ for transformation temperatures ($\alpha(M_s) = 7$ MPa K^{-1} and $\alpha(M_f) = 15$ MPa K^{-1} for initial polycrystals in tension; $\alpha(M_s) = -12$ MPa K^{-1} and $\alpha(M_f) = -60$ MPa K^{-1} for initial polycrystals in compression) result in MT temperature intervals increase with the growth of applied stress. The behavior of temperature intervals at forward $\Delta_1 = M_s - M_f$ and reverse

$\Delta_2 = A_f - A_s$ MT can be described according to (2)–(5) as well as the thermal hysteresis, defined as the difference between temperatures $\frac{M_s+M_f}{2}$ and $\frac{A_s+A_f}{2}$. The elastic and dissipative energies at forward and reverse MT are assumed to be the same at similar volume fraction of oriented martensite ξ: $e_{\xi=0}^{A\to M} = e_{\xi=0}^{M\to A} = e_{\xi=0}$; $e_{\xi=1}^{A\to M}(\xi) = e_{\xi=1}^{M\to A}(\xi) = e_{\xi=1}(\xi)$; $d_{\xi=0}^{A\to M} = d_{\xi=0}^{M\to A} = d_{\xi=0}$; $d_{\xi=1}^{A\to M}(\xi) = d_{\xi=1}^{M\to A}(\xi) = d_{\xi=1}(\xi)$, therefore temperature intervals would be written as follows:

$$\Delta_1 (M_s - M_f) = \frac{e_{\xi=1}(\xi) + d_{\xi=1}(\xi) - e_{\xi=0} - d_{\xi=0}}{-\Delta s}, \quad (6)$$

$$\Delta_2 (A_f - A_s) = \frac{e_{\xi=1}(\xi) - d_{\xi=1}(\xi) - e_{\xi=0} + d_{\xi=0}}{-\Delta s}, \quad (7)$$

$$\Delta T = \frac{d_{\xi=0} + d_{\xi=1}(\xi)}{-\Delta s}. \quad (8)$$

Figures 5 and 6 illustrate that thermal hysteresis ΔT, which is determined by dissipative energy during MT (8) and does not change significantly with applied stress growth; increased ΔT is observed only when irreversibility is taking place in $\varepsilon(T)$ curves at high applied stress. Appearance of irreversibility is evidence of increased dissipative energy. So, the tension/compression asymmetry of thermal hysteresis after SIM-aging is absent as well as in initial polycrystals.

Furthermore, MT Δ_1 and Δ_2 temperature intervals will increase with martensite volume fraction.

Temperature intervals increase with applied stress is evidence of increased elastic energy, which is caused by both a high density of compound twins and detwinning processes. It is known [18] that in NiTiHf systems the B19′-martensite possess a high density of compound (001) twins, which are not the solution of crystallographic theory of MT and appear as geometrically necessary twins in regions with high elastic stress and for compatibility between matrix deformation and the elastic strain of nanosized particles in TiNi-based alloys (figure 1). On the one hand, these twins appear according to large size of Hf atoms, which strongly distort the crystal lattice providing elastic stresses. On the other hand, nanosized dispersed H-phase particles are also the reason for twins appearance [18]. Martensite crystal detwinning under stress results in significantly increased elastic energy that impedes MT to cause, reduces M_f and A_s transformation temperatures, and ultimately widens temperature intervals.

At the same time, temperature intervals Δ_1 and Δ_2 demonstrate greater increase following SIM-aging in comparison with initial state. Such behavior is observed in compression and in tension as well.

First, during the stress-induced formation of oriented martensite in SIM-aged crystals the total stress level is higher than in initial state, because internal stresses presented in SIM-aged crystals act as an external one. So, the higher total stress level in SIM-aged crystals effects stronger on the internal twinning structure of martensite in comparison with initial state. Therefore, SIM-aged crystals at high applied stress $\sigma \geqslant 300$ MPa, demonstrated substantially wider temperature intervals of forward and reverse MTs as well as the II type of MT [33] with $A_s < M_s$ in comparison with initial crystals, where the I type of MT ($A_s > M_s$) was observed (figure 4). Similar behavior and $A_s < M_s$ are expected in initial state at higher applied stress, as has been observed in $Ni_{50.3}Ti_{29.7}Hf_{20}$ polycrystals [9].

Second, SIM-aging leads to viscoelastic property change. Stress-free oriented martensite growth following SIM-aging provides an increase of elastic modulus that is indirectly evidenced by increased strength properties, as it follows from [32]. Increased elastic modulus in turn results in significant growth of elastic energy, which is defined by the difference of elastic moduli between austenite and martensite [34].

Third, the change of transformation entropy obtained by DSC curves (table 1) effects on temperature intervals. Previous research demonstrated that SIM-aging in Heusler alloys results in decreased transformation entropy [30, 31] and according to (2)–(8), such entropy reduction provides for increased temperature intervals in SIM-aged crystals in comparison with initial state.

4. Conclusions

In the present study, the effect of SIM-aging in tension and compression on one-way and TWSME in NiTiHf polycrystals containing nanosized *H*-phase particles was investigated. SIM aging was conducted at 428 K for 12 h under tensile and compressive stresses of 300 MPa and −400 MPa, respectively.

Key experimental results and conclusions are summarized as follows:

(a) SIM-aging is an effective way to induce the fully reversible TWSME with strain up to 50% of one-way shape memory strain in NiTiHf polycrystals. High-temperature TWSME strain in tension reached 2.3% without any additional training.
(b) SIM-aging altered material viscoelastic properties: an increase of elastic moduli of both phases as well as internal friction was observed. It is assumed that increased compatibility between *H*-phase particles and twinned martensite structure during SIM-aging provides for interface mobility increase, which promotes internal friction growth.
(c) Reduced M_f and A_s transformation temperatures, and consequently the increase of MT temperature intervals in cooling/heating cycles at any applied stress level, were observed due to increased elastic energy during MT following SIM-aging. Such an increase of elastic energy is caused by several factors: increased elastic moduli, increased compatibility between particles and martensite, and the difficulty of martensite detwinning.

Acknowledgments

This work was supported by the Ministry of Education and Science of the Russian Federation, Project No. 0721-2020-0022.

ORCID iD

A I Tagiltsev https://orcid.org/0000-0002-6824-6846

References

[1] Karaca H E, Saghaian S M, Ded G, Tobe H, Basaran B, Maier H J, Noebe R D and Chumlyakov Y I 2013 Effects of nanoprecipitation on the shape memory and material properties of a Ni-rich NiTiHf high temperature shape memory alloy *Acta Mater.* **61** 7422–31

[2] Hayrettin C, Karakoc O, Karaman I, Mabe J H, Santamarta R and Pons J 2019 Two way shape memory effect in NiTiHf high temperature shape memory alloy tubes *Acta Mater.* **163** 1–13

[3] Stebner A P *et al* 2014 Transformation strains and temperatures of a nickel–titanium–hafnium high temperature shape memory alloy *Acta Mater.* **76** 40–53

[4] Tsuchiya K, Tateyama K, Sugino K and Marukawa K 1995 Effect of aging on the rubber-like behavior in Cu-Zn-Al martensites *Scr. Metall. Mater.* **32** 259–64

[5] Otsuka K and Ren X 2001 Mechanism of martensite aging effects and new aspects *Mater. Sci. Eng.* A **312** 207–18

[6] Timofeeva E E, Panchenko E Y, Pichkaleva M V, Tagiltsev A I and Chumlyakov Y I 2018 The effect of stress-induced martensite ageing on the two-way shape memory effect in $Ni_{53}Mn_{24}Ga_{22}$ single crystals *Mater. Lett.* **228** 490–2

[7] Niendorf T, Krooß P, Somsen C, Eggeler G, Chumlyakov Y I and Maier H E 2015 Martensite aging—an avenue to new high temperature shape memory alloys *Acta Mater.* **89** 298–304

[8] Eftifeeva A, Yanushonite E, Panchenko E and Chumlyakov Y 2018 Effect of stress-assisted ageing in austenite and martensite on two-way shape memory effect in [001]-oriented $Co_{35}Ni_{35}Al_{30}$ single crystals *AIP Conf. Proc.* **2051** 020071

[9] Sehitoglu H, Wu Y, Patriarca L, Li G, Ojha A, Zhang S, Chumlyakov Y and Nishida M 2017 Superelasticity and shape memory behavior of NiTiHf alloys *Shape Memory Superelasticity* **3** 168–87

[10] Chen X, Chen W, Ma Y, Zhao Y, Deng C, Peng X and Fu T 2020 Tension-compression asymmetry of single-crystalline and nanocrystalline NiTi shape memory alloy: an atomic scale study *Mech. Mater.* **145** 103402

[11] Zhang J, Xul Y, Otsuka K, Ren X, Chumlyakov Y and Asai M 2003 Orientation dependence of stress-induced martensitic transformation in quenched Ti-50. 8at%Ni single crystals *J. Physique* IV **112** 669–72

[12] Bigelow G S, Garg A, Padula II S A, Gaydosha D J and Noebe R D 2011 Load-biased shape-memory and superelastic properties of a precipitation strengthened high-temperature $Ni_{50.3}Ti_{29.7}Hf_{20}$ alloy *Scr. Mater.* **64** 725–8

[13] Saghaian S M, Karaca H E, Souri M, Turabi A S and Noebe R D 2016 Tensile shape memory behavior of $Ni_{50.3}Ti_{29.7}Hf_{20}$ high temperature shape memory alloys *Mater. Des.* **101** 340–5

[14] Ma J, Karaman I and Noebe R D 2010 High temperature shape memory alloys *Int. Mater. Rev.* **55** 257–315

[15] Coughlin D R, Casalena L, Yang F, Noebe R D and Mills M J 2016 Microstructure–property relationships in a high-strength 51Ni–29Ti–20Hf shape memory alloy *J. Mater. Sci.* **51** 766–78

[16] Yang F, Coughlin D R, Phillips P J, Yang L, Devaraj A, Kovarik L, Noebe R D and Mills M J 2013 Structure analysis of a precipitate phase in an Ni-rich high-temperature NiTiHf shape memory alloy *Acta Mater.* **61** 3335–46

[17] Han X D, Wang R, Zhang Z and Yang D Z 1998 A new precipitate phase in a TiNiHf high temperature shape memory alloy *Acta Mater.* **46** 273–81

[18] Santamarta R, Arroyave R, Pons J, Evirgen A, Karaman I, Karaca H E and Noebe R D 2013 TEM study of structural and microstructural characteristics of a precipitate phase in Ni-rich Ni–Ti–Hf and Ni–Ti–Zr shape memory alloys *Acta Mater.* **61** 6191–206

[19] Canadinc D, Trehern W, Ozcan H, Hayrettin C, Karakoc O, Karaman I, Sun F and Chaudhry Z 2017 On the deformation response and cyclic stability of $Ni_{50}Ti_{35}Hf_{15}$ high temperature shape memory alloy wires *Scr. Mater.* **135** 92–96

[20] Miura N, Zhang J, Ren X, Otsuka K, Suzuki T, Tanaka K, Chumlyakov Y and Asai M 1999 Elastic softening of $Ti_{49.2}Ni_{50.8}$ single crystal prior to B2–B19′ martensitic transformation *Proc. Int. Conf. on Solid-Solid Phase Transformations 1999* pp 827–30

[21] Zhang J, Xue D, Cai X, Ding X, Ren X and Sun J 2016 Dislocation induced strain glass in $Ti_{50}Ni_{45}Fe_5$ alloy *Acta Mater.* **120** 130–7

[22] Shuitcev A, Li L, Markova G V, Golovin I S and Tong Y X 2020 Internal friction in $Ti_{29.7}Ni_{50.3}Hf_{20}$ alloy with high temperature shape memory effect *Mater. Lett.* **262** 127025

[23] Nembach E 1997 *Particle Strengthening of Metals and Alloys* (New York: Wiley) p 285

[24] Atli K C, Karaman I, Noebe R D, Bigelow G and Gaydosh D 2015 Work production using the two-way shape memory effect in NiTi and a Ni-rich NiTiHf high-temperature shape memory alloy *Smart Mater. Struct.* **24** 125023

[25] Kustov S, Pons J, Cesari E and Van Humbeeck J 2004 Chemical and mechanical stabilization of martensite *Acta Mater.* **52** 4547–59

[26] Kockar B, Karaman I, Kim J I and Chumlyakov Y 2006 A method to enhance cyclic reversibility of NiTiHf high temperature shape memory alloys *Scr. Mater.* **54** 2203–8

[27] Karakoc O, Hayrettin C, Evirgen A, Santamarta R, Canadinc D, Wheeler R W, Wang S J, Lagoudas D C and Karaman I 2019 Role of microstructure on the actuation fatigue performance of Ni-Rich NiTiHf high temperature shape memory alloys *Acta Mater.* **175** 107–20

[28] Umale T, Salas D, Tomes B, Arroyave R and Karaman I 2019 The effects of wide range of compositional changes on the martensitic transformation characteristics of NiTiHf shape memory alloys *Scr. Mater.* **161** 78–83

[29] Saghaian S M, Karaca H E, Tobe H, Turabi A S, Saedi S, Saghaian S E, Chumlyakov Y I and Noebe R D 2017 High strength NiTiHf shape memory alloys with tailorable properties *Acta Mater.* **134** 211–20

[30] Tóth L Z, Daróczi L, Panchenko E, Chumlyakov Y and Beke D L 2020 Acoustic emission characteristics and change the transformation entropy after stress-induced martensite stabilization in shape memory $Ni_{53}Mn_{25}Ga_{22}$ single crystal *Materials* **13** 2174

[31] Beke D L, Daróczi L, Samy N M, Tóth L Z and Bolgár M K 2020 On the thermodynamic analysis of martensite stabilization treatments *Acta Mater.* **200** 490–501

[32] Tagiltsev A I, Panchenko E Y, Chumlyakov Y I, Fatkullin I D and Karaman I 2020 Two-way shape memory effect in stress-induced martensite aged $Ni_{50.3}Ti_{32.2}Hf_{17.5}$ alloy *Mater. Lett.* **268** 127589

[33] Otsuka K 1998 *Shape Memory Materials* (Cambridge: Cambridge University Press)

[34] Liu Y and Yang H 1999 The concern of elasticity in stress-induced martensitic transformation in NiTi *Mater. Sci. Eng.* A **260** 240–5